Model Development of Flexible Disk Grinding Process

Song-Min Yoo*, Myung-Jin Choi, Young-Jin Kim
College of Mechanical and Industrial System Engineering, Kyung Hee University

A flexible disk grinding process model was developed based on the dynamic relationship proposed by Kurfess and the influence of the major system parameters which potentially affect the grinding process was studied. Due to the process complexities, several new parameters were assumed to be kinematically dependent on the geometric layouts of the process. Different process stages had been defined depending on the kinematic relationships between the grinding disk and workpiece. A trend of depth of cut was simulated using the proposed model and compared with the empirically measured data in two dimensions. Due to a poor prediction capability of the first model, a modified model was proposed and a better performance has been proved to reveal a closer description of processed surface quality. Also a deflection length has been verified using a different analytical approach.

Key Words : Flexible Disk, Process Stages, Deflection Length, Disk Orientation Angle, Depth of Cut

1. Introduction

A grinding process as a surface finishing technique plays an important part in the production process for obtaining high machining accuracy, consistent product quality and good the surface roughness of the workpiece. It is used to enhance the surface finish quality both in size and shape. Despite of its importance as a final process with a high level of quality and precision, it is one of the least understood processes. Kegg (1983) emphasized the importance of developing an improved understanding of the grinding process from the perspective of modeling, control and optimization. Among those categories, modeling has been recognized as one of the least developed areas due to process complexity and uncertainty of its parameters and several efforts have been focused on the process parameter identification and monitoring with proper sensing systems.

As for modeling of the grinding process, a series of studies were made to determine and to understand the influence of grinding process parameters. As static characteristics among the process parameters, wheel characteristics have often been studied. Approximate formula of the elasticity modulus of the grinding wheels had been described and its influence on force and stock removal rate was identified (Spur and Stark, 1984; Ikuse and Unno, 1999). Grinding wheel profiles were obtained by using a convolution of random waves (Sathyanarayanan, 1985) and a continuous time series model (Pandit and Wu, 1973). König (1982) used a numerical method to describe the workpiece topography over a contact length with the grinding wheel. A process simulation model using a single grit wheel was implemented by Dornfeld (1981) to observe the effect of various rake angles. Overall wheel parameters such as grit size, concentration and binder modulus were related to chip thickness and area providing guidelines for choosing wheel specification (Miller and Dow, 1999).

Other modeling studies have been using various process related parameters. The surface finish was

* Corresponding Author,
E-mail : smyoo@khu.ac.kr
TEL : +82-31-201-2579 ; **FAX** : +82-31-202-8106
College of Mechanical and Industrial System Engineering, Kyung Hee University, Yongin-si, 1, Kyungki-do 449-701, Korea.(Manuscript **Received** April 27, 2000 ; **Revised** July 1, 2000)

studied for stock removal rates by Lindsay and Hahn (1971). Process parameters such as feed rate and depth of cut were correlated with force and stock removal rate by Pahlizsch (1970). Malkin (1987) studied method to obtain the maximum stock removal rate with limited machine power, minimum wheel wear and thermal damage. A grinding force and power could be related to the dressing operation by considering the effective density of the cutting edge on the wheel surface(Chen et al, 1999). The grinding process is also limited by constraints such as machine power capacity, tool vibration, thermal damage, wheel wear and surface finish (King and Hahn, 1986). Methodologies producing the best output quality within the 0.375 μm(King and Hahn, 1986) to 0.6 μm(Malkin, 1987) Ra range while obtaining maximum stock removal rate (Malkin and Koren, 1980) were studied.

Dynamic modeling of the grinding process involves process control. Jenkins et al. (1997) developed a linear grinding model relating normal force to material removal rate. Grinding tool path model using vision camera was developed (Park et al., 2000). A plunge grinding with cupped aluminum oxide wheel was used to process low carbon steel. Kurfess (1987) had developed a force-vision controlled robotics grinding system in order to remove weld bead, a task commonly used in the automotive and shipbuilding industries, and in the automatic grinding task of cast iron stamping dies. Even though an analytical model was developed and verified, it was limited to a certain workpiece surface. In this model, a grinding wheel was put in the grinder mount which was pivoted at one end and was connected by a spring at the other end to the milling machine quill. Since the whole grinder mount rotates around the pivot, the location of the grinding wheel spinning axis also varies during the process causing compliance effect. Similar studies involving tool deflection could often be found in the processes like end milling (Seo and Cho, 1999).

In this study, an analytical model of the grinding process using a flexible disk as a grinding wheel is briefly outlined and modified. Kinematic relationships of the process is defined based on the geometric disposition of the tool and workpiece. In this model, surface profile process output referring to the surface quality is simulated using the proposed process model. The performance of the simulation is evaluated by comparison with the empirical data.

2. General Model

Figure 1 displays a descriptive diagram of the grinding process using flexible disk. The disk is continuously deflected due to the infeed action of the workpiece during the process. A grinding disk attached to a rubber platen was used as the tool. Since Kurfess's model was developed with an assumption that the spinning axis is free to rotate, it is not an adequate model of the process used in this study. Figure 2 shows the grinding process schematic during introduced in this study. The basic assumption of the model is that the static model in Fig. 2 holds for every time interval, Δt. It was also assumed that the disk spinning axis deflection is small and negligible compared to the disk deflection with respect to the disk center, G. Dynamic relationships developed by Kurfess using a force and moment balance was applied to the model in Fig. 2 leading to the following nonlinear first order differential equation which represents disk rotational angular velocity.

$$\dot{\alpha} = -\frac{v_{fx}\sin\alpha}{R_s} + \frac{1}{A_r R_s}[k_1 w \mu K_s(\alpha_0 - \alpha) - k_2] \tag{1}$$

where α_0 : initial disk orientation angle
α : current disk angle
$\dot{\alpha}$: disk rotational angular velocity

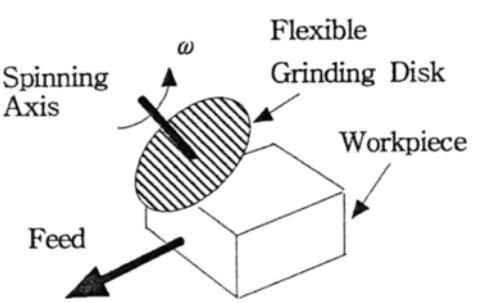

Fig. 1 Flexible Disk Grinding Process

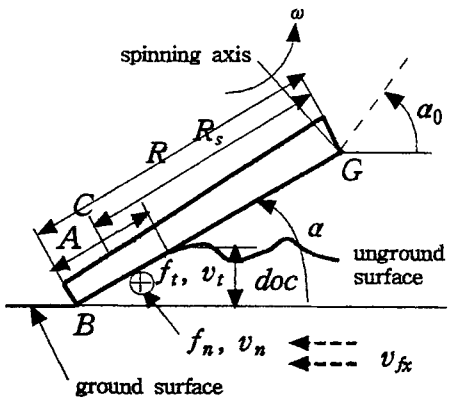

Fig. 2 Grinding Process Schematis

μ : frictional coefficient between the disk and the workpiece
K_s : torsional spring constant of disk
R_s : distance from disk center to contact area center (effective radius)
v_{fx} : feed velocity
w : wheel velocity
$A_r(=AD)$: contact area between the disk and the workpiece
k_1, k_2 : constants
A : length of the disk in contact with workpiece (contact length)
D : thickness of the workpiece

Equation (1) incorporates several values that can be found experimentally from an actual grinding pass. The location of the disk tip B, (from which the surface or depth of cut profile will be determined, relative to the disk center G can be found as follows from the kinematic relationships shown in Fig. 2.

$$x=R\cos\alpha \qquad (2)$$
$$y=R\sin\alpha$$

where

x : disk tip location in horizontal coordinate
y : disk tip location in vertical coordinate
R : Disk radius

Therefore, the depth of cut can be related with the location of the disk tip point B found in Eq. (2). The trace of the depth of cut constitutes the processed surface profile.

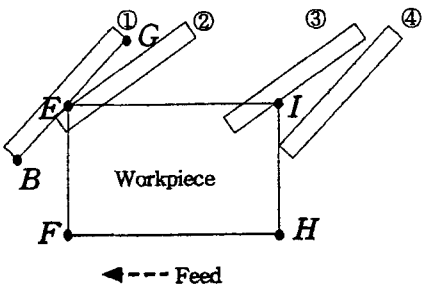

Fig. 3 Grinding process stages

R_s and A_r are to be updated from the geometric relationships. Contrary to the Kurfess' assumption, all kinematic relationships change depending on the layout between the disk and the workpiece. In other words, since Kurfess model has defined only the dynamic behaviour of the process, processed surface profiles could be hardly regenerated without the knowledge of kinematic relationships between the process parameters. Therefore, different kinematic relationships have to be developed to provide various calculation routines for A_r and R_s. The solution of Eq. (1) produces a complete output profile of the flexible disk grinding process. The output profile is produced and considered only when the disk tip is in contact with the workpiece.

3. Process Stages

Several process parameters including A_r and R_s have to be updated from the grinding process geometry. Considering the grinding process with rectangular workpiece $E\ F\ H\ I$ and initial disk angle $\alpha_0(0°<\alpha_0<90°)$ with respect to $E\ F$, the grinding process can be divided into 3 stages which are defined as in Fig. 3:

1) Entrance stage : Transitional stage from the initial contact (E is on the line BG) between the disk and the workpiece until disk tip B is fully embedded in the workpiece (B is on the line EF) or from disk position ① to disk position ② in Fig. 3

2) Between edges stage : Stage from the end of the entrance stage until the disk begins to leave the workpiece (I is on the line BG) or from disk position ② to disk position ③ in Fig. 3

3) Exit stage : Transitional stage from the end

of the between edges stage until the disk leaves the workpiece (B is on the line HI) or from disk position ③ to disk position ④ in Fig. 3

The following condition is required for the existence of the between edges stage.

$$\overline{EI} > \frac{doc_{b0}}{\tan\alpha_{b0}} \tag{3}$$

where

$\overline{EI}$: distance from E to I

doc_{b0} : depth of cut at the beginning of the between edges stage

α_{b0} : disk angle at the beginning of the between edges stage

Even though the above classification has been drawn with respect to a rectangular (flat top surface) specimen, the same rules can be applied for a specimen with an arbitrary surface profile.

3.1 Entrance stage

Figure 4 shows the detailed model geometry at the entrance stage. The rectangle $EFHI$ represents the workpiece. As the grinding proceeds, the disk center moves from A to R_s and the disk begins to be deflected. The development to find A and R_s starts with determining CD as:

$$\overline{CD_b} = \frac{h}{\tan\alpha_0} + v_{fx}t_b \tag{4}$$

$$h = R\sin\alpha_0 - doc_0 \tag{5}$$

where

$\overline{CD_b}$: distance from disk center G' (current location of the disk center) to front face line EF

h : distance from disk center to specimen top surface

t_b : time passed since the beginning of entrance stage

doc_0 : initial depth of cut

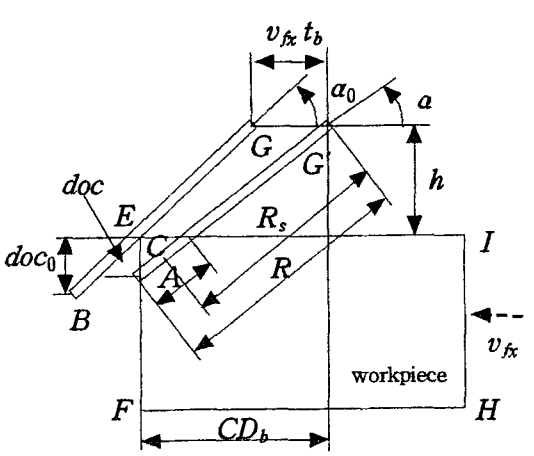

Fig. 4 Geometry of entrance stage

Contact length A and effective radius R_s are

$$A = \frac{\overline{CD_b}}{\cos\alpha} - \frac{h}{\sin\alpha} \tag{6}$$

$$R_s = \frac{h}{\sin\alpha} + \frac{A}{2} \tag{7}$$

From Eqs. (4)-(7)

$$R_s = \frac{h}{2\sin\alpha} + \frac{1}{2\cos\alpha}\left(\frac{h}{\tan\alpha_0} + v_{fx}t_b\right) \tag{8}$$

Now, all the grinding process parameter values can be updated with Eqs. (1) and (4)-(7). In the entrance stage, the disk cuts the left-most side of the workpiece and the disk tip has not yet reached the workpiece. Therefore, no surface output profile is formed. The last updated process parameter values in this stage will be used as initial conditions for the next between edges stage where output depth of cut profiles are initiated.

3.2 Between edges stage

Once the disk tip is in contact with the workpiece, A and R_s are simply expressed as (Fig. 4)

$$A = R - \frac{h}{\sin\alpha} \tag{9}$$

$$R_s = \frac{A}{2} + \frac{h}{\sin\alpha} = \frac{R}{2} + \frac{h}{2\sin\alpha} \tag{10}$$

The depth of cut, doc, which is directly related with output surface profile can be found from the disk geometry as

$$doc = R\sin\alpha - h \tag{11}$$

3.3 Exit stage

As a final stage of the process, the exit stage is where the deflected status of the disk is restored to the original configuration because of decreasing contact length A. Figure 5 displays the geometry of the exit stage. A and R_s can be derived as follows:

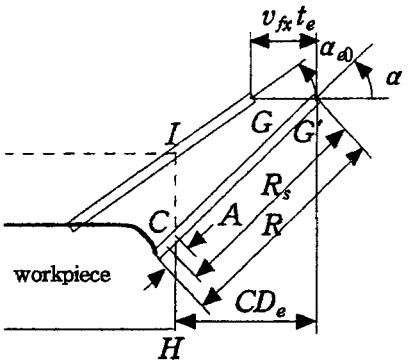

Fig. 5 Geometry of exit stage

$$\overline{CD_e}=\frac{h}{\tan\alpha_{e0}}+v_{fx}t_e \tag{12}$$

where

CD_e : distance from current disk center G' to end face line HI

α_{e0} : angle at the beginning of the exit stage

t_e : time passed since the beginning of the exit stage

And

$$A=R-\frac{\overline{CD_e}}{\cos\alpha}=R-\frac{1}{\cos\alpha}\left(\frac{h}{\tan\alpha_e}+v_{fx}t_e\right) \tag{13}$$

Then R_s is found as

$$R_s=R-\frac{A}{2}=\frac{R}{2}+\frac{1}{2\cos\alpha}\left(\frac{h}{\tan\alpha_{e0}}+v_{fx}t_e\right) \tag{14}$$

The expression for the depth of cut is the same as in Eq. (11).

4. Experiment and Result

4.1 Apparatus

A 3M brand 120 grain disk (type C, closed coat and aluminum oxide) was attached to a 177.8 mm diameter rubber platen used as the grinding wheel. This wheel was attached to the vertical milling machine spindle. The vertical spindle axis was aligned with an inclination with respect to the workpiece surface to provide proper flexibility of the disk. The output surface profile was measured by a separate optical scanning system.

4.2 Experiment and results

In order to check the validity of the model, a wood specimen with 50 mm width and height ($\overline{EI}$ and $\overline{EF}$ in Fig. 3) made of oak was used. The 10 mm thickness was employed for the specimen to eliminate the lateral dimension effect of the disk and to prevent breakage and serious lateral deflection during the process due to the tangential force component, f_t. The depth of cut was 12. 7 mm for this specimen. The depth of cut is rather large compared with that used in practice. A larger value was assumed since it would be suitable for model evaluation as the transition stage is more evident. A system constant, K_s was obtained from the disk bending test while μ, k_1,k_2 were derived from the relationships between the cutting force component and the supplied power.

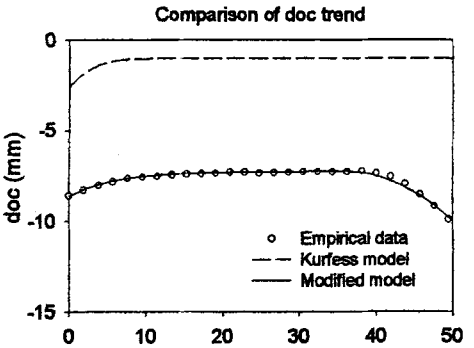

Fig. 6 Comparison of doc trend

As can be seen in Fig. 6, there is a significant difference between the results of the experiment and the simulation. A smaller depth of cut and higher profile level is shown in the simulated output profile compared to the actual measurement due to a smaller predicted contact area. In order to understand the cause of the above discrepancy, the trend of the disk tip angle during the grinding process was monitored. The grinding disk was stopped in the middle of the process and the specimen was removed from the milling machine mount. The disk tip angle α measured from the workpiece using a gauge still represented a gap between the simulation and experiment.

5. Modified Model

The inadequacy of the previous results require that an improved model be developed. A new assumption for the disk deflection for the im-

proved model development is that the grinding disk tip was actually deflected locally around the middle of its radial span contrary to the previous assumption that the disk is deflected with respect to the disk center. Figure 7 shows the modified grinding process model. A new variable, d_f (deflection arm distance, deflection length), representing the distance from the deflection point, J, to the disk tip, B, has been introduced (Fig. 7).

5.1 Development

A force and moment balance was applied to the model proposed in Fig. 7 and the following relationships were derived:

$$v_n = v_{fx}\sin\alpha + \dot{\alpha}R_{sm} \tag{15}$$

$$m = f_n R_{sm} = K_s(\alpha_0 - \alpha) \tag{16}$$

$$P = f_t v_t = w\mu K_s(\alpha_0 - \alpha)\frac{R_s}{R_{sm}} \tag{17}$$

where v_t : tangential velocity component
v_n : normal velocity component
m : moment
f_t : tangential force component
f_n : normal force component
P : supplied power

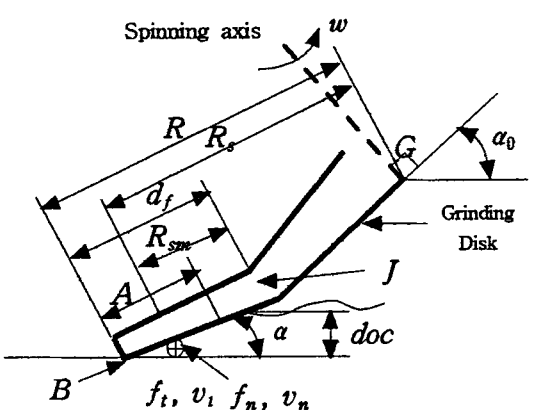

Fig. 7 Modified model schematic diagram

R_{sm} is the distance from the deflection center, J, to the contact length center, C, expressed as

$$R_{sm} = d_f - \frac{A}{2} \tag{18}$$

From Eqs. (15)-(17) Eq. (1) is modified as

$$\dot{\alpha} = -\frac{v_{fx}\sin\alpha}{R_{sm}} + \frac{1}{A_r R_{sm}}\left[k_1 w\mu K_s(\alpha_0 - \alpha)\frac{R_s}{R_{sm}} - k_2\right] \tag{19}$$

The process output profile can be simulated using the modified equations. Same process stages and equations defined earlier can be also applied to the modified model. In Eqs. (6)-(14), R and R_s are substituted with d_f and R_{sm} since the deflection center has changed from G to J in Fig. 7.

5.2 Results and discussions

It has been observed that the depth of cut was maintained at a constant level during the between edges stage. To find the proper value of d_f, the steady-state depth of cut (the constant depth of cut in the between edges stage) was represented with respect to various values of d_f (Fig. 8). The actual depth of cut and α from the experiment were 7.3 mm and 28.6°, respectively, while the corresponding d_f was found to be 33.4 mm as shown in Fig. 8. Another simulation was done using Eqs. (15)-(17) and the d_f value. In Fig. 6, a good correspondence between the experiment and the simulation using the revised model is shown.

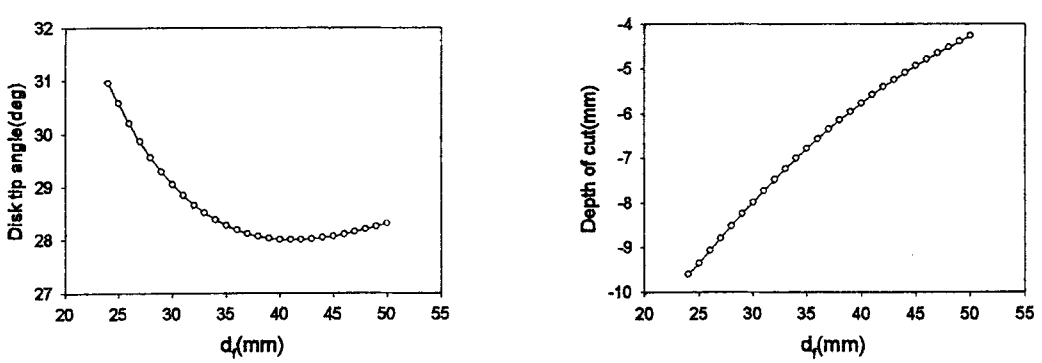

Fig. 8 Trend of steady state α and doc

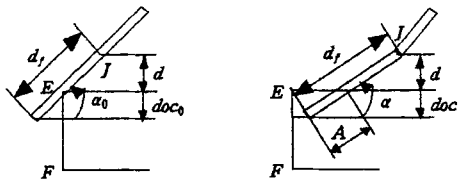

(a) $t=0$ (b) Between edges stage

Fig. 9 Modified model description

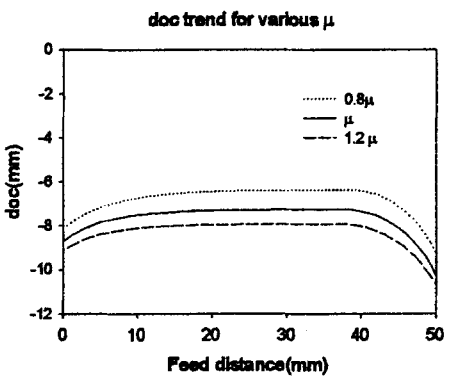

Fig. 10 doc trend for various μ

The value of d_f can also be verified in a different manner. Figure 9 shows two different geometries of the disk at the initial entrance time t_0(disk position ① in Fig. 3) and at the between edges stage. These positions lead to the following relations.

$$\sin\alpha_0\left(d_f-\frac{doc_0}{\sin\alpha_0}\right)=d \tag{20}$$

$$d_f-\frac{d}{\sin\alpha}=A \tag{21}$$

where

d : distance from the workpiece surface to the deflection center J

The only unknown variables are d_f and d in Eqs. (20) and (21). Therefore by eliminating d from both equations, an expression for d_f can be found as

$$d_f=\frac{doc_0-A\sin\alpha}{\sin\alpha_0-\sin\alpha} \tag{22}$$

The d_f found in Eq. (22) matches the value from Fig. 8 which verifies the validity of the modified model.

Figures 10 and 11 display the trend of depth of

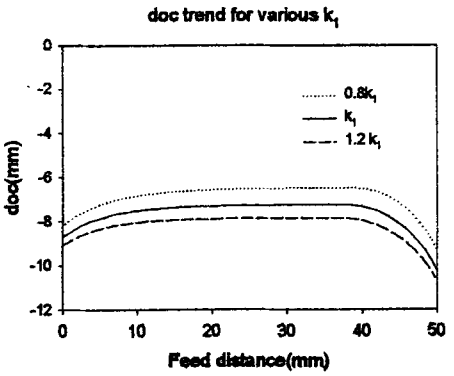

Fig. 11 doc trend for various k_1

cut for various μ and k_1. Higher value for each parameter corresponds to heavier grinding, and therefore, show deeper depth of cut.

6. Conclusions

It was observed that the Kurfess' model was not sufficient enough to represent the grinding process with flexible disk. Therefore, a modified model including the local disk deflection length, d_f, and three different process stages was introduced. It was observed that the modified model predicted the output depth of cut profile which corresponded well to the actual process result.

A separate routine to verify the validity of d_f was developed.

Since the process parameters such as μ, k_1 and K_s change depending on the specimen characteristics such as type of disk material, disk dimension and grinding wheel wear condition, those parameters should be adjusted accordingly.

References

Chen, X., Rowe, W. B., Allanson, D. R. and Mills, B., 1999, "A Grinding Power Model for Selection of Dressing and Grinding Conditions," *Trans. of the ASME, J. of Manu. Sci. and Eng.*, Vol. 121, pp. 632~637.

Dornfeld, D. A., 1981, "Single Grit Simulation of the Abrasive Machining of Wood," *Trans. ASME, J. Eng. Ind.*, Vol. 103, No. 1, pp. 1~12.

Ikuse, Y. and Unno, K., 1999, "Study on

Deducing Elastic Modulus of Super Abrasive Grinding Wheel Using Acoustic Model," *J. of the Japan Soc. for Prec. Eng.*, Vol. 65, No. 8, pp. 1174~1179.

Jenkins, H. E., Kurfess. T. R. and Ludwick, S. J., 1997, "Determination of a Dynamic Grinding Model," *Trans of ASME, J. of Dyn. Sys. Measurement & Control*, Vol. 119, No. 2, pp. 289~293.

Kegg, R. L., 1983, "Industrial problems in grinding," *Annals of the CIRP*, Vol. 32, No. 2, pp. 559~561.

King, R. I. and Hahn, R. S., 1986, *Handbook of Modern Grinding Technology*, Chapman and Hall, New York.

König, W., 1982 "A Numerical Method to Describe the Kinematics of Grinding," *Annals of the CIRP*, Vol. 31, No. 1, pp. 201~204.

Kurfess, T. R., 1987, "Verification of a Dynamic Grinding Model," MIT Mechanical Eng. M. S. Thesis.

Lindsay, R. P. and Hahn, R. S., 1971, "On the Basic Relationship Between Grinding Parameters," *Annals of the CIRP*, Vol. 19, No. 4, pp. 657~664

Malkin, S. and Koren, Y., 1980, "Off-line Grinding Optimization with a Micro-Computer," *Annals of the CIRP*, Vol. 29, No. 1, pp. 213~216

Malkin, S., 1987, "Practical Grinding Optimization," *Proc. 15th NAMRC, SME*, Lehigh Univ., Bethlehem Pennsylvania, pp. 123~140.

Miller, M. H. and Dow, T. A., 1999, "Influence of the Grinding Wheel in the Ductile Grinding of Brittle Materials: Development and Verification of Kinematic Based Model," *Trans. of ASME, J. of Manufact. Sci. & Eng.*, Vol. 121, No. 4, pp. 638~646.

Pahlizsch, G., 1970, "Internationaler Atand der Forschung auf dem Gebiet des Schleifen von Holtz," Holz als Roh- und Werkstoff, Vol. 28, No. 9, pp. 329~343

Pandit, S. M. and Wu, S. M., 1973, "Characterization of Abrasive Tools by Continuous Time Series," *Trans. ASME, J. Eng. Ind.*, Vol. 95, No. 1, pp. 821~825.

Park, K. W., Lee, J. H., Oh, B. O. and Lee, M. K., 2000, "Development of Robot Control and Measurement for Unknown Geometric Surface Grinding," *Trans. of the KSME*, Vol. 24, No. 4, pp. 1039~1046 (In Korean).

Sathyanarayanan, G., 1985, "Two Wavelength Characteristic Grain Model for Grinding Wheel," *Annals of the CIRP*, Vol. 34, No. 1, pp. 299~303.

Seo, T. I. and Cho, M. W., 1999, "Tool Trajectory Generation Based on Tool Deflection Effects in the Flat-End Milling Process (II) -Prediction and Compensation of Milled Surface Error," *KSME Int'l J.*, Vol. 13, No. 12, pp. 918~930.

Spur, G. and Stark, C., 1984, "Method for Grinding Wheel Quality," *Proc. 12th NAMRC*, SME, Houghton, Michigan, pp. 339~346.